Power Electronics and Drives
Volume 10(45), 2025 DOI: 10.2478/pead-2025-0002

sciendo

Power Electronics and Drives

An Improved SOGI-Higher-Order Sliding Mode Observer-Based Induction Motor Speed Estimation

Research paper

Kobena Badu Enyam[1,*], Francis Boafo Effah[1], Desmond Hammond[2]

[1]Kwame Nkrumah University of Science and Technology, Kumasi, Ghana, Department of Electrical/Electronic Engineering
[2]Ecole Centrale de Nantes, Nantes, France, Department of Electrical Engineering

Received: 08 September 2024; Accepted: 22 November 2024

Abstract: This article presents a novel adaptive gain tuning second-order generalised integrator (SOGI)-higher-order sliding mode (HOSM) observer for robust speed estimation for an induction motor's entire speed range. This article introduces a hyperbolic tangent function and a varying gain exponent that ensures accurate speed estimation under noisy conditions and significantly reduces chattering observed in conventional sliding mode observers (SMOs). The robustness of the proposed speed estimation method is verified through simulations conducted on MATLAB/Simulink R2024a developed by MathWorks, demonstrating its capability to effectively track the motor's actual speed even under varying load torque conditions, parameter variations and additional sensor noise. The proposed approach's superiority and robustness were compared with the conventional SOGI-frequency locked loop (FLL) and super twisting algorithm (STA) SMO.

Keywords: *induction machine • second-order generalised integrator • super twisting algorithm • higher-order sliding mode • speed estimation*

1. Introduction

Precise speed data is crucial for precise speed regulation in induction motor drives. An encoder or a direct speed sensor is typically required to measure the speed of the motor. Nevertheless, employing direct speed sensors undermines the intrinsic durability and efficiency of the motor, necessitating supplementary electronics, wiring, space, regular maintenance and meticulous installation. Moreover, this increases the cost of the drive system (Holtz, 1998, 2002; Ilas et al., 1994). As a result of these difficulties, there has been a notable shift in research towards the creation of alternative indirect approaches. Therefore, there is significant interest among researchers in constructing high-performance induction motor drives that can operate without the need for direct speed sensors. This can be referred to as the development of speed-sensorless induction motor drives. These drives provide several benefits, such as less hardware complexity, reduced costs, smaller size, elimination of direct sensor wire, improved noise immunity, enhanced dependability and decreased maintenance needs (Zaky et al., 2009).

Earlier methods for speed estimation relied on non-ideal phenomena, such as signal injection (Caruana et al., 2006; Gao et al., 2007; Leppanen and Luomi, 2006) and rotor slot harmonic extraction (Gao et al., 2011; Raute et al., 2010; Zhao et al., 2015). While these methods are effective across a wide speed range and are resistant to parameter variations, they can introduce unwanted side effects in induction motor drives, such as significant torque ripples and unnecessary power losses (Holtz, 2006). Additionally, challenges in signal extraction and limited flexibility reduce their practical applicability.

In power systems, synchronisation is commonly achieved using synchronous reference frame-phase-locked loops (SRF-PLLs) to accurately determine grid voltage components' phase, frequency and amplitude (Golestan et al., 2016, 2017). Their effectiveness in estimating speed for sensorless motor drive control (Wang et al., 2012, 2013)

* Email: kobena.enyam@ashesi.edu.gh, kobenaenyam@gmail.com

has driven significant research into SRF-PLL-based technologies. However, SRF-PLLs encounter difficulties in suppressing disturbances such as harmonics, DC offsets and parameter variations, which can lead to inaccuracies in estimation. As a result, ongoing developments have focused on enhancing the ability of SRF-PLLs to attenuate these disturbances, thereby improving the precision of parameter estimation.

The second-order generalised integrator (SOGI) speed observers present an alternative for sensorless speed estimation in induction motors (Wang et al., 2021). The SOGI method theoretically picks up the fundamental frequency of Electromotive force (before integration. SOGI speed observer methods proposed in the literature have been capable of removing most of the speed estimator problems mentioned above. However, new issues of poor speed estimation at low speeds and during frequency ramps are to be expected (Bouzidi et al., 2022; Xin et al., 2016; Zhao et al., 2016). To address the observability issue at low speeds and during frequency ramps, third-order, fourth-order and cascade generalised integrators were proposed (Bamigbade and Khadkikar, 2022; Wang et al., 2021; Xin et al., 2016), which significantly increase the complexity of the estimator. Despite using intricate cascade SOGI configurations for speed estimation, experimental results show that speed estimation deviations can still occur at very low speeds due to the filter’s heightened sensitivity to DC values when the speed approaches zero (Hao and Luo, 2024).

The sliding mode observer (SMO) is the most commonly employed sensorless control approach among the methods mentioned. This is mainly owing to its notable features, such as a straightforward algorithm, resilience to parameter fluctuations and impressive dynamic performance. However, as identified in previous studies (Khoshhava et al., 2021; Mansouri et al., 2020), the conventional SMO has two significant drawbacks: first, the chattering phenomenon, resulting from a constant observer gain, which negatively impacts estimation accuracy. Second, the accuracy of the rotor speed and position estimates is decreased by high-order harmonics and external noise in the fundamental back-EMF estimation, particularly in dynamic settings. To solve the above-mentioned problems, authors have introduced improved versions of the SMO (Farahat et al., 2024) introduced an improved SOGI-SMO using a sigmoid function; the proposed scheme performs satisfactorily under motor faulty conditions. However, speed estimation during transient periods was not the best due to increased harmonics, especially DC offsets. An adaptive gain super-twisting SMO was proposed by Nurettin and İnanç (2023) to eliminate the chattering in SMOs, the proposed scheme performed very well at low speeds, however the tuning of multiple gains for every operating condition does not guarantee stability of all the time. The improved SMO introduced by Sun et al. (2024), performed poorly under additional sensor noise and parameter variation as much burden was placed on the controller to reduce chattering. A voltage model observer based on SMO was proposed by Wang et al. (2024) to solve the issue of DC offsets causing speed estimation degradation; even though speed estimation at various speed ranges was very good, further improvements are needed for robust speed estimation at low speeds.

Given the deficiencies noted above, this work aims to provide the following contributions: proposing an improved combined SOGI-higher-order sliding mode (SOGI-HOSM) observer for accurate speed estimation of an induction motor across its entire speed range. This is achieved by introducing a variable gain exponent to improve the observer’s robustness even in the presence of sensor measurement noise and parameter variations and a hyperbolic tangent function to reduce chattering significantly.

The remaining portion of the article is structured into the subsequent sections: Section 2 provides in-depth details of the modelling of the direct vector control approach for the motor controller design, where the proposed novel adaptive gain tuning SOGI-HOSM will be deployed in the feedback loop as a substitute for an encoder. Section 3 explains the modelling of the conventional SOGI-frequency locked loop (FLL) method. Section 4 focuses on modelling the conventional super-twisting algorithm (STA). Section 5 provides a detailed explanation of the modelling of the proposed novel adaptive gain tuning SOGI-HOSM. Section 6 explains the stability analysis of the proposed method. Section 7 details the results and simulations conducted in MATLAB/Simulink.

2. Vector Control Approach for Induction Motor Control Design

Field-oriented control (FOC) is a widely adopted technique for the precise control of induction motors, offering independent regulation of flux and torque (Traore et al., 2007). This method transforms the three-phase stator currents into a rotating reference frame aligned with the rotor flux. Doing so decouples the stator current’s flux and torque components, mimicking a DC motor’s control structure, where field and armature currents are independently managed. The outcome is enhanced control accuracy, particularly beneficial for applications demanding high-performance variable-speed motor drives.

2.1. Coordinate transformation and rotating reference frame

To achieve decoupling, the stator currents i_a, i_b and i_c are first transformed into two orthogonal components: the d-axis (aligned with the rotor flux) and the q-axis (responsible for torque production). This transformation is accomplished in two steps:

- The Clarke transformation converts the three-phase system into two stationary components ($\alpha\beta$ reference frame).
- The Park transformation then converts these stationary components into the rotating dq reference frame.

The d-axis current, i_{sd}, corresponds to the flux-producing component, while the q-axis current, i_{sq}, governs the torque production. This decoupling enables the flux and torque to be controlled independently, providing an efficient means for motor control similar to a DC machine.

2.2. Stator voltage equations in the dq reference frame

In the dq reference frame, the stator voltage equations describe the relationship between the stator currents, rotor flux and the angular velocity of the system. These equations are:

$$\begin{aligned} v_{sd} &= i_{sd}R_s + \sigma L_s \frac{d}{dt} i_{sd} - \omega_e \sigma L_s i_{sq} + \frac{L_m}{L_r}\frac{d}{dt}\phi_{rd} \\ v_{sq} &= i_{sq}R_s + \sigma L_s \frac{d}{dt} i_{sq} + \omega_e \sigma L_s i_{sd} + \omega_e \frac{L_m}{L_r}\phi_{rd} \end{aligned} \tag{1}$$

where

- v_{sd}, v_{sq} are the d-axis and q-axis stator voltages, respectively,
- i_{sd}, i_{sq} are the d-axis and q-axis stator currents,
- R_s is the stator resistance and σL_s is the leakage inductance,
- L_m is the mutual inductance and L_r is the rotor inductance and
- ϕ_{rd} is the rotor flux aligned with the d-axis.

These equations demonstrate how the stator currents contribute to the overall stator voltage, considering the mutual and leakage inductances. Importantly, the q-axis current directly influences the torque production, while the d-axis current controls the rotor flux.

2.3. Rotor voltage equations and rotor flux orientation (RFO)

In vector control, the rotor flux is often oriented along the d-axis RFO, simplifying the rotor voltage equations. Under these conditions, the q-axis rotor flux component (ϕ_{rq}) becomes zero, reducing the complexity of the rotor voltage equations. The resulting rotor equations are:

$$\begin{aligned} 0 &= \frac{R_r}{L_r}\phi_{rd} - \frac{L_m}{L_r} R_r i_{sd} + \frac{d}{dt}\phi_{rd} \\ 0 &= -\frac{L_m}{L_r} R_r i_{sq} + \omega_{sl}\phi_{rd} \end{aligned} \tag{2}$$

where

- R_r is the rotor resistance
- ω_{sl} is the slip frequency, representing the difference between synchronous and rotor speeds.

The first equation links the rotor flux to the d-axis stator current, while the second equation highlights the role of the q-axis stator current in determining the slip frequency. The slip frequency is directly proportional to the q-axis stator current, responsible for torque production.

2.4. Slip frequency and torque production in vector control

The slip frequency (ω_{sl}) is a critical parameter in vector control as it directly influences the motor's torque. It is proportional to the q-axis stator current $\left(i_{sq}\right)$ and the magnetising current $\left(i_{mrd}\right)$:

$$\omega_{sl} = \frac{R_r}{L_r i_{mrd}} i_{sq} = k_{sl} i_{sq} \tag{3}$$

Here, k_{sl} the slip gain depends on the rotor resistance, inductance and magnetising current. The magnetising current $\left(i_{mrd}\right)$ is responsible for generating the rotor flux, defined as:

$$\phi_{rd} = L_m i_{mrd} \tag{4}$$

The motor torque (T) is then proportional to the product of the q-axis stator current and the magnetising current:

$$T = kL_m i_{sq} i_{mrd} \tag{5}$$

where

- T is the motor torque,
- L_m is the mutual inductance and
- k is a constant that varies depending on the scaling convention.

2.5. Decoupling of flux and torque control

The d-axis stator current (i_{sd}) governs the rotor flux, while the q-axis stator current (i_{sq}) is responsible for torque generation. This decoupling allows for high dynamic performance and precise control.

The magnetising current i_{mrd} is derived from the d-axis current and remains responsible for establishing the rotor flux, while the q-axis current directly controls the torque. The final control equations for the d-axis and q-axis under RFO are:

- For the d-axis (flux control):

$$\frac{L_r}{R_r} \frac{d}{dt} i_{mrd} + i_{mrd} = i_{sd} \tag{6}$$

- For the q-axis (torque control):

$$\omega_{sl} = \frac{R_r}{L_r i_{mrd}} i_{sq} \tag{7}$$

These equations demonstrate that the d-axis current primarily controls the magnetising current, while the q-axis current determines the slip frequency and torque. The motor torque is given in Eq. (5).

2.6. Direct rotor flux orientation (DRFO)

In DRFO (Jansen and Lorenz, 1993), the rotor flux angle, θ, is derived by estimating the rotor flux from stator measurements (stator voltages and currents) in the stationary reference frame (denoted as the αβ frame). These measurements calculate the rotor flux and its orientation ϕ, allowing for precise motor control.

The dynamic equations of the stator coils in the $\alpha\beta$ frame can be written as:

$$\begin{aligned} v_{s\alpha} &= i_{s\alpha} R_s + \frac{d}{dt}\phi_{s\alpha} \\ v_{s\beta} &= i_{s\beta} R_s + \frac{d}{dt}\phi_{s\beta} \end{aligned} \tag{8}$$

where $v_{s\alpha}$ and $v_{s\beta}$ are the stator voltages, $i_{s\alpha}$ and $i_{s\beta}$ are the stator currents, R_s is the stator resistance and $\phi_{s\alpha}$ and $\phi_{s\beta}$ are the stator flux linkages.

The rotor flux components in the $\alpha\beta$ frame can be expressed in terms of stator and rotor currents:

$$\begin{aligned} \phi_{r\alpha} &= L_r i_{r\alpha} + L_m i_{s\alpha} \\ \phi_{r\beta} &= L_r i_{r\beta} + L_m i_{s\beta} \end{aligned} \tag{9}$$

where L_r is the rotor inductance, L_m is the mutual inductance and $i_{r\alpha}, i_{r\beta}$ are the rotor currents. By integrating the stator voltage equations and utilising the rotor flux relationships, the rotor flux angle θ is derived as:

$$\theta = \tan^{-1}\left(\frac{\phi_{r\beta}}{\phi_{r\alpha}}\right) \tag{10}$$

This angle θ represents the orientation of the rotor flux in space and is critical for controlling the stator currents to regulate torque and speed.

Integrator drift occurs when flux estimation based on the integration of stator voltages is affected by small DC offsets or noise, causing errors in the calculated flux angle over time, particularly at low frequencies. The accuracy of flux estimation is also highly sensitive to variations in stator resistance, R_s, which fluctuates with temperature and operating conditions. This sensitivity becomes especially problematic at low speeds, amplifying errors in the flux calculation. As a result, the performance of DRFO control significantly degrades below 2 Hz, where the combined effects of integrator drift and R_s sensitivity make flux estimation unreliable, potentially preventing the motor from starting. Details on the Proportional Integral (PI) controller design for the implemented vector control method in Figure 1 is given in Echeikh et al. (2016).

3. Conventional SOGI-FLL

The SOGI-FLL is a method of adaptive filtering used to estimate several properties of a single-phase voltage, such as frequency, amplitude, orthogonal components and phase angle. This approach is beneficial since it can effectively filter harmonics and requires low processing resources. The SOGI-FLL system comprises two main constituents: the SOGI and the FLL. The SOGI is a filter that generates two voltage components, vα and vβ, which are in-phase and quadrature-phase, respectively, corresponding to the input voltage V_{in}. The FLL determines the angular frequency (ω) of the input voltage V_{in}, which is subsequently utilised to fine-tune the SOGI filter for the best efficiency.

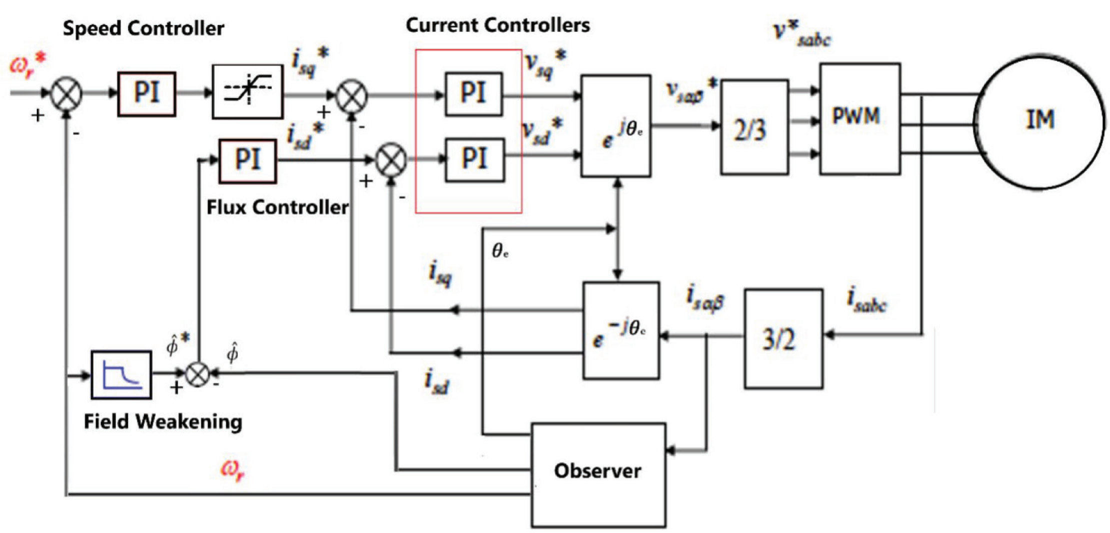

Figure 1. Block diagram of induction machine sensorless control scheme of the DRFO method. DRFO, direct rotor flux orientation.

The SOGI operates as a band-pass filter (BPF) for vα and as a low-pass filter (LPF) for vβ, with their corresponding mathematical equations defined in Bouzidi et al. (2022):

$$v_\alpha(s) = \frac{k\omega s}{s^2 + k\omega s + \omega^2} v_{\text{in}}(s) \tag{11}$$

$$v_\beta(s) = \frac{ks}{s^2 + k\omega s + \omega^2} v_{\text{in}}(s)$$

The selection of the gain k for the SOGI is based on finding a suitable compromise between achieving a rapid dynamic response and ensuring efficient harmonic filtering performance. Furthermore, the frequency calculated by the SOGI-FLL can be expressed as:

$$\omega = -\frac{\gamma}{s}\left(v_{in}(s) - v_\alpha(s)\right)v_\beta(s) \tag{12}$$

where the FLL gain (described below) is represented by γ.

$$\gamma = \frac{k\omega_o}{V^2}\Gamma \tag{13}$$

V represents the estimated amplitude, whereas Γ is a positive gain that relies on the settling time of the FLL.

4. Conventional STA

The STA is considered a HOSM algorithm, particularly a second-order type, and is described by the general formulation outlined below (Polyakov and Poznyak, 2009):

$$\begin{cases} \dot{\hat{x}}_1 = f(\hat{x}_2) + k_1 |e_1|^{0.5} \operatorname{sign}(e_1) + \rho_1 \\ \dot{\hat{x}}_2 = k_2 \operatorname{sign}(e_1) + \rho_2 \end{cases} \tag{14}$$

where $y_1 = \hat{x}_1$, $e_1 = y_1 - \hat{y}_1, x_i$ are the state variables, k_1 and k_2 are the observation gains, ρ_1 and ρ_2 are the perturbation terms.

The observer equations, after being applied to the induction machine, are given as:

$$\dot{\hat{i}}_{\alpha,s} = \zeta_\alpha - \gamma \hat{i}_{\alpha,s} + \frac{\hat{v}_{\alpha,s}}{\text{Ls}\sigma} + K_{1,\alpha}\sqrt{|\tilde{i}_{\alpha,s}|}\operatorname{sign}(\tilde{i}_{\alpha,s}) \tag{15}$$

$$\text{where } \zeta_\alpha = K\,\hat{\omega}_r \hat{\phi}_{\beta,r} + \frac{K\hat{\phi}_{\alpha,r}}{\tau_r} \tag{16}$$

$$\text{Substituting } K = K_\alpha \text{: } K_\alpha = \frac{\tau_r \zeta_\alpha}{\hat{\phi}_{\alpha,r} + \hat{\omega}_r \hat{\phi}_{\beta,r} \tau_r} \tag{17}$$

$$\dot{\zeta}_\alpha = K\dot{\hat{\omega}}_r \hat{\phi}_{\beta,r} + \hat{\omega}_r \dot{\hat{\phi}}_{\beta,r} + \frac{K\dot{\hat{\phi}}_{\alpha,r}}{\tau_r} + K_{2,\alpha}\operatorname{sign}(\tilde{i}_{\alpha,s}) \tag{18}$$

$$\dot{\zeta}_\alpha = K\left(\dot{\hat{\omega}}_r \hat{\phi}_{\beta,r} + \hat{\omega}_r \dot{\hat{\phi}}_{\beta,r}\right) + \frac{K\dot{\hat{\phi}}_{\alpha,r}}{\tau_r} + K_{2,\alpha}\operatorname{sign}(\tilde{i}_{\alpha,s})$$

$$\dot{\hat{i}}_{\beta,s} = \zeta_\beta - \gamma \hat{i}_{\beta,s} + \frac{\hat{v}_{\beta,s}}{\text{Ls}\sigma} + K_{1,\beta}\sqrt{|\tilde{i}_{\beta,s}|}\operatorname{sign}(\tilde{i}_{\beta,s}) \tag{19}$$

$$\text{where } \zeta_\beta = \frac{K\hat{\phi}_{\beta,r}}{\tau_r} - K\hat{\omega}_r\,\hat{\phi}_{\alpha,r} \tag{20}$$

$$\text{Substituting } K = K_\beta\text{: } K_\beta = \frac{\tau_r\,\zeta_\beta}{\hat{\phi}_{\beta,r} - \hat{\omega}_r\,\hat{\phi}_{\alpha,r}\,\tau_r} \tag{21}$$

$$\dot{\zeta}_\beta = \frac{K\dot{\hat{\phi}}_{\beta,r}}{\tau_r} - K\left(\dot{\hat{\omega}}_r\,\hat{\phi}_{\alpha,r} + \hat{\omega}_r\dot{\hat{\phi}}_{\alpha,r}\right) + K_{2,\beta}\,\mathrm{sign}\left(\tilde{i}s_{\beta,s}\right) \tag{22}$$

By equating $K_\alpha = K_\beta$:

$$\frac{\tau_r\,\zeta_\alpha}{\hat{\phi}_{\alpha,r} + \hat{\omega}_r\hat{\phi}_{\beta,r}\,\tau_r} = \frac{\tau_r\,\zeta_\beta}{\hat{\phi}_{\beta,r} - \hat{\omega}_r\hat{\phi}_{\alpha,r}\,\tau_r}$$

$$\text{The estimated speed is given as: } \hat{\omega}_r = \frac{\hat{\phi}_{\beta,r}\,\zeta_\alpha - \hat{\phi}_{\alpha,r}\,\zeta_\beta}{\hat{\phi}_{\beta,r}\,\tau_r\,\zeta_\beta + \hat{\phi}_{\alpha,r}\,\tau_r\,\zeta_\alpha} \tag{23}$$

Rotor fluxes are derived as follows:

$$\dot{\hat{\phi}}_{\alpha,r} = \frac{\mathrm{Lm}\hat{i}_{\alpha,s}}{\tau_r} - \frac{\hat{\phi}_{\alpha,r}}{\tau_r} - \hat{\omega}_r\hat{\phi}_{\beta,r}$$

$$\dot{\hat{\phi}}_{\beta,r} = \hat{\omega}_r\,\hat{\phi}_{\alpha,r} - \frac{\hat{\phi}_{\beta,r}}{\tau_r} + \frac{\mathrm{Lm}\hat{i}_{\beta,s}}{\tau_r}$$

It can also be expressed as:

$$\dot{\hat{\phi}}_{\alpha,r} = \frac{\mathrm{Lm}\hat{i}_{\alpha,s}}{\tau_r} - \zeta_\alpha \tag{24}$$

$$\dot{\hat{\phi}}_{\beta,r} = \frac{\mathrm{Lm}\hat{i}_{\beta,s}}{\tau_r} - \zeta_\beta \tag{25}$$

Estimated load torque is given by:

$$\hat{T}_{load} = -\frac{2J\dot{\hat{\omega}}_r - p\hat{T}_e + B\,p\hat{\omega}_r}{p} \tag{26}$$

where

$$\hat{T}_e = \frac{3p}{2}\left(\hat{i}_{\beta,s}\hat{\phi}_{\alpha,r} + \hat{i}_{\alpha,s}\hat{\phi}_{\beta,r}\right) \tag{27}$$

5. Improved Adaptive Gain Exponent SOGI-HOSM Observer

5.1. SOGI

Due to the excellent filtering capabilities, the SOGI topology is employed to filter out vα and $v\beta$ as shown below:

$$\hat{v}_\alpha(s) = \frac{k\omega s}{s^2 + k\omega s + \omega^2}v_{\mathrm{in}}(s)$$

$$\hat{v}_\beta(s) = \frac{ks}{s^2 + k\omega s + \omega^2}v_{\mathrm{in}}(s) \tag{28}$$

where ω represents the resonance frequency of the SOGI

5.2. Modelling of proposed adaptive gain tuning HOSM observer

In conventional super twisting observers, the correction term which is the sliding mode reaching law includes a discontinuous reaching law, often includes a signum function to enforce convergence to the sliding surface. However, due to the abrupt nature of the sign function:

$$\mathrm{Sign}(e)=\begin{cases}1, & e>0\\ -1, & e<0\end{cases}$$

Chattering occurs, which can affect the observer and consequently control performance.

To mitigate chattering, the sign function is replaced with a hyperbolic tangent function $\tanh(e/\gamma)$, where e is the error signal and γ is a tunable parameter providing flexibility in controlling the steepness of the tanh slope, hence smoothness of the switching, especially important at low error values (i.e. $|$ noise $+e|<1$). This smoother transition prevents abrupt switching, leading to stable and accurate state estimations. By dynamically tuning γ (ranging from 0.01 to 1), the observer can adapt to different conditions: Larger $\gamma, \tanh(e/\gamma)$ smooths and reduces the steepness of the transition around $e=0$, reducing oscillations in low-error scenarios, As $\gamma \to 0, \tanh(e/\gamma) \to \mathrm{Sign}(e)$ provides faster responses. A sweet spot must be chosen experimentally between Super Twisting Observer's robustness and performance.

To address sensitivity to measurement noise, typical in super twisting SMO algorithms identified in literature and noise introduced by parameter variations and integrated drift issues introduced because of the direct vector control approach utilised in this article, a modified observer is proposed with a tunable gain exponent parameter α, which adjusts based on the noise level magnitude. In literature, α is set to 0.5 for super-twisting observers (Ammar et al., 2024) and α is set to 1 for high-gain observers (Veluvolu and Soh, 2009). The proposed HOSM seeks to vary α from 0.5 to 1 depending on the noise magnitude estimated in the current sensor. The proposed HOSM formulation is described below:

$$\begin{cases}\dot{z}_1 = z_2 + g_1(u(t)) + K_1\mu\left|e_{1_n}\right|^{\alpha}\tanh\left(e_{1_n}/\gamma\right)\\ \dot{z}_2 = f_s(y_n, u(t)) + L\left(\dot{z}_2, g_2(u(t))\right) + K_2\alpha\mu^2\left|e_{1_n}\right|^{2\alpha-1}\tanh\left(e_{1_n}/\gamma\right)\\ \alpha = \left(1+e^{\left(\lambda-0.5\left(1+\frac{z_3^q}{z_3^q+0.1q}\right)\right)}\right)^{-1}\\ \dot{z}_3 = -\tau z_3 + \tau\left|x_n hf(t)\right|\end{cases} \tag{29}$$

where

- $\hat{z}_1, \hat{z}_2$ are the observer state variables,
- $\hat{z}_3$ is a first-order LPF of $\left|x_{nhf}(t)\right|$,
- e_{1_n} represents the difference (error) between the observer's estimation and the true state, z_1, in the presence of noise,
- α: is the output of the sigmoid function, representing the adjusted gain factor in the observer,
- z_3 is the state variable associated with noise and disturbance in the system,
- q is an exponent that modulates the influence of the noise or disturbance on the gain factor α,
- λ is a bias term allowing fine-tuning of the response,
- τ is a constant parameter chosen sufficiently low to keep the frequency range of the low pass filter z_3 sufficiently low,
- ϵ_2 is a constant parameter chosen to keep alpha between 0.5 and 1 and
- The high-frequency component of the current sensor, denoted as $\left|x_{nhf}(t)\right|$, is derived by applying a high-pass Butterworth filter.

The proposed observer equation as applied to the induction machine is given as:

$$\dot{\hat{i}}_{\alpha,\mathrm{s}} = \zeta_\alpha - \gamma\hat{i}_{\alpha,s} + \frac{\hat{v}_{\alpha,s}}{\mathrm{Ls}\sigma} + K_{1,\alpha}\,\mu_\alpha\left|\tilde{i}_{\alpha,s_n}\right|^{\alpha}\tanh\left(\tilde{i}_{\alpha,s_n}\right) \tag{30}$$

$$\text{where } \zeta_{\alpha} = K\hat{\omega}_r\hat{\phi}_{\beta,r} + \frac{K\hat{\phi}_{\alpha,r}}{\tau_r} \tag{31}$$

$$\text{Substituting } K = K_{\alpha}\text{: } K_{\alpha} = \frac{\tau_r\,\zeta_{\alpha}}{\hat{\phi}_{\alpha,r} + \hat{\omega}_r\,\hat{\phi}_{\beta,r}\,\tau_r} \tag{32}$$

$$\dot{\zeta}_{\alpha} = K\dot{\hat{\omega}}_r\hat{\phi}_{\beta,r} + \hat{\omega}_r\dot{\hat{\phi}}_{\beta,r} + \frac{K\dot{\hat{\phi}}_{\alpha,r}}{\tau_r} + K_{2,\alpha}\,\mu_{\alpha}{}^{2}\left|\tilde{i}_{\alpha,s_n}\right|^{2\alpha-1}\tanh\left(\tilde{i}_{\alpha,s_n}\right) \tag{33}$$

$$\dot{\zeta}_{\alpha} = K\left(\dot{\hat{\omega}}_r\hat{\phi}_{\beta,r} + \hat{\omega}_r\dot{\hat{\phi}}_{\beta,r}\right) + \frac{K\,\dot{\hat{\phi}}_{\alpha,r}}{\tau_r} + K_{2,\alpha}\,\mu_{\alpha}{}^{2}\left|\tilde{i}_{\alpha,s_n}\right|^{2\alpha-1}\tanh\left(\tilde{i}_{\alpha,s_n}\right)$$

$$\dot{\hat{i}}_{\beta,s} = \zeta_{\beta} - \gamma\,\hat{i}_{\beta,s} + \frac{\hat{v}_{\beta,s}}{\mathrm{Ls}\,\sigma} + K_{1\beta,}\,\mu_{\alpha}\left|\tilde{i}_{\beta,s_n}\right|^{\alpha}\tanh\left(\tilde{i}_{\beta,s_n}\right) \tag{34}$$

$$\zeta_{\beta} = \frac{K\hat{\phi}_{\beta,r}}{\tau_r} - K\hat{\omega}_r\,\hat{\phi}_{\alpha,r} \tag{35}$$

$$\text{Substituting K} = K_{\beta}\;\; K_{\beta} = \frac{\tau_r\,\zeta_{\beta}}{\hat{\phi}_{\beta,r} - \hat{\omega}_r\,\hat{\phi}_{\alpha,r}\,\tau_r} \tag{36}$$

$$\dot{\zeta}_{\beta} = \frac{K\dot{\hat{\phi}}_{\beta,r}}{\tau_r} - K\left(\dot{\hat{\omega}}_r\hat{\phi}_{\alpha,r} + \hat{\omega}_r\dot{\hat{\phi}}_{\alpha,r}\right) + K_{2,\beta}\,\mu_{\beta}{}^{2}\left|\tilde{i}_{\beta,s_n}\right|^{2\alpha-1}\tanh\left(\tilde{i}_{\beta,s_n}\right) \tag{37}$$

Again, speed is estimated as given in Eqs (23) and (24).

$$\dot{\mathrm{z}}_{noise} = -\tau\mathrm{z}_{noise} + 0.5\tau\left|i_{\alpha,s_{nhf}}(t) + i_{\beta,s_{nhf}}(t)\right| \tag{38}$$

The variables $i_{\alpha k_{nhf}}(t)$ and $i_{\beta k_{nhf}}(t)$ represent the filtered high-frequency component of the current sensor output.

6. Stability Analysis of the Proposed Adaptive Gain Exponent SOGI-HOSM Observer

The stability analysis of the proposed SOGI-HOSM observer is based on the framework introduced in Ghanes et al. (2022). The observer's stability is established using the error dynamics, defined as:

$$\tilde{Z} = \begin{bmatrix} \tilde{z}_1 \\ \tilde{z}_2 \end{bmatrix} = \begin{bmatrix} z_1 - \tilde{z}_1 \\ z_2 - \tilde{z}_2 \end{bmatrix} \tag{39}$$

where $\tilde{z}_1$ and $\tilde{z}_2$ represent the differences between the actual and estimated states. The derivative of the error dynamics is given by:

$$\dot{\tilde{Z}} = \begin{bmatrix} \tilde{z}_2 - K_1\left|\tilde{z}_1\right|^{\alpha}\tanh\left(\tilde{z}_1\right) \\ F\left(t,\tilde{z}_1,\tilde{z}_2\right) - K_2\left|\tilde{z}_2\right|^{2\alpha-1}\tanh\left(\tilde{z}_2\right) \end{bmatrix} \tag{40}$$

Here, $F\left(t,\tilde{z}_1,\tilde{z}_2\right)$ is a Lebesgue measurable perturbation term. This term is bounded as $F\left(t,\tilde{z}_1,\tilde{z}_2\right) \le \tilde{F}_{\max}$, where $\tilde{F}_{\max}$ is a constant upper bound. The perturbation spectrum primarily contains low-frequency components, ensuring mathematical and practical feasibility.

To analyse stability, a Lyapunov candidate function is defined as:

$$V = \tilde{\mathbf{Z}}^{T}P\tilde{\mathbf{Z}} \tag{41}$$

where P is a positive definite matrix. The derivative of V is computed as:

$$\dot{V} = \tilde{z}_1\tilde{z}_2 + \tilde{z}_2 F\left(t,\tilde{z}_1,\tilde{z}_2\right) - K_1\left|\tilde{z}_1\right|^{\alpha+1} - \frac{K_2\tilde{z}_2\left|\tilde{z}_2\right|^{2\alpha}\tanh\left(\tilde{z}_2\right)}{\left|\tilde{z}_2\right|}$$

For the error to decrease over time, the following conditions for K_1 and K_2 must be satisfied:

$$K_1 = -\frac{\tilde{z}_1\tilde{z}_2}{\left|\tilde{z}_1\right|^{\alpha+1}},\ K_2 = \frac{\tilde{z}_1\left|\tilde{z}_2\right| + \left|\tilde{z}_2\right| F\left(t,\tilde{z}_1,\tilde{z}_2\right)}{\left|\tilde{z}_2\right|^{2\alpha}\tanh\left(\tilde{z}_2\right)} \tag{42}$$

The adaptive gains K_1 and K_2 depend on the signs of $\tilde{z}_1$ and $\tilde{z}_2$:

1. If $\tilde{z}_1 < 0, K_1 = \frac{\tilde{z}_1\tilde{z}_2}{\left(-\tilde{z}_1\right)^{\alpha+1}}$ and if $\tilde{z}_1 \geq 0, K_1 = \frac{\tilde{z}_1\tilde{z}_2}{\tilde{z}_1^{\alpha+1}}$.
2. If $\tilde{z}_2 < 0, K_2 = \frac{\tilde{z}_2\left(\tilde{z}_1 + F\left(t,\tilde{z}_1,\tilde{z}_2\right)\right)}{\left(-\tilde{z}_2\right)^{2\alpha}}$ and if $\tilde{z}_2 > 0, K_2 = \frac{\tilde{z}_2\left(\tilde{z}_1 + F\left(t,\tilde{z}_1,\tilde{z}_2\right)\right)}{\tilde{z}_2^{2\alpha}}$.

The following conditions ensure stability:

- $\tilde{z}_1 + F\left(t,\tilde{z}_1,\tilde{z}_2\right) > 0$
- Non-zero noise levels: $\left|\tilde{z}_1\right|,\left|\tilde{z}_2\right| \neq 0$.
- Perturbation term satisfies $\|F\|_{\min} \neq 0$.

The Lyapunov analysis ensures that the observer states converge under bounded perturbations and noise. The adaptive gains K_1 and K_2 dynamically compensate for variations in noise and system parameters, ensuring robustness. The conditions highlight the importance of bounded perturbations ($F_{\max}$) and accurate gain adaptation to maintain stability. Large deviations in noise levels or inaccuracies in gain tuning could challenge stability, particularly if $F\left(t,\tilde{z}_1,\tilde{z}_2\right)$ approaches its upper bound. However, the proposed dynamic adaptation mechanism mitigates these risks, ensuring that the Lyapunov derivative remains negative and stability is preserved.

7. Results and Discussion

The Simulink/MATLAB programme was utilised to model the adaptive gain tuning method proposed on an induction motor model. The speed reference was provided in the form of variable speed commands. A much more sophisticated speed reference was designed with the MATLAB/Simulink signal builder package to properly assess the performance of the compared speed estimation methods. The parameters used for design of the induction motor model is given in Table 1. A varying load torque shown in Figure 2, was used throughout all simulation scenarios to assess the performance of the compared speed estimation schemes. The robustness of the evaluated speed estimation methods was assessed by calculating the speed estimation error, which represents the difference between the real speed and the estimated speed.

The motor parameters used in the simulation are given below:

Table 1. Parameters of Induction motor model used.

Motor parameters	Values
R_s	2.3
L_s	0.261 H
L_r	0.261 H
P	4
B	0.0286 kg · m^{-2}
J	0.02 kg · m^{-2}

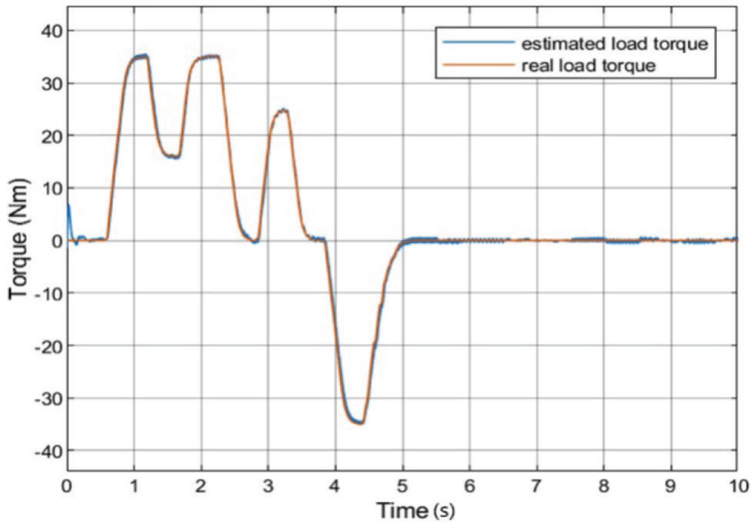

Figure 2. Varying load torque.

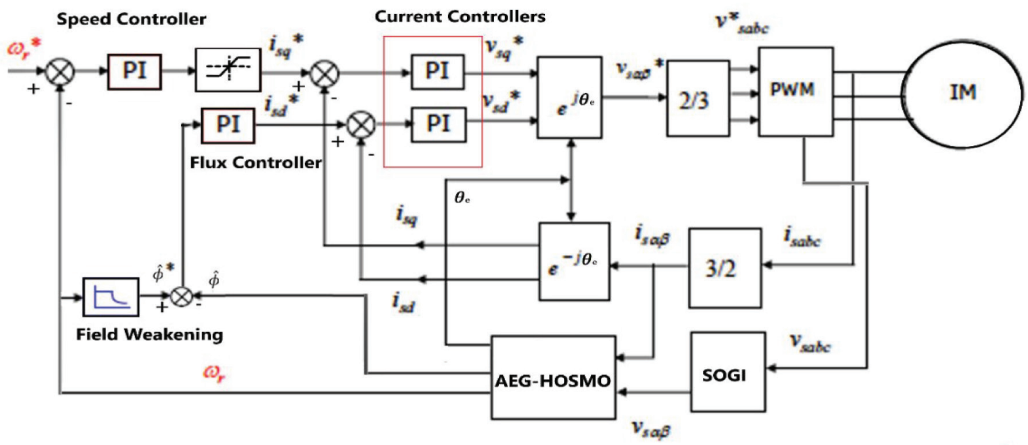

Figure 3. Block diagram of Induction machine sensorless control scheme with proposed SOGI-HOSM. SOGI-HOSM, second-order generalised integrator-higher-order sliding mode.

The speed estimation capabilities of the conventional STA, the SOGI-FLL and the proposed SOGI-HOSM were compared by placing each in the feedback loop of the direct vector control approach detailed in Section 2 and Figure 1. The direct vector control approach with the proposed SOGI-HOSM system is shown in Figure 3. Theoretically, ϕ_{rq} must be zero to achieve complete decoupling; however, in practical applications, the q-axis rotor flux ϕ_{rq} is not expected to be precisely zero but should remain within a small range. In this case, ϕ_{rq} as shown in Figure 4 oscillates between approximately −0.05 and 0.05, indicating effective decoupling. These minor oscillations are within acceptable limits and reflect adequate alignment with the rotor flux, suggesting that the vector control system achieves practical decoupling. The electromagnetic torque estimated due to effective decoupling is shown in Figure 5.

In Figure 6, the stator voltages in the Pulse Width Modulation (PWM) inverter-fed machine are of a PWM nature, containing high-frequency components from the switching harmonics. To extract the fundamental component essential for control, the SOGI is employed. The SOGI acts as a BPF for the in-phase component (Vα) and a LPF for the quadrature component (Vβ), effectively isolating the fundamental frequency from high-frequency PWM harmonics. This filtered output provides the control system with clean, low-frequency stator voltage signals, critical for accurate estimation and reliable control.

However, the SOGI introduces a phase delay due to its filtering action. The proposed HOSM is used to compensate for this delay. This observer dynamically adjusts its gain exponent α based on detected noise levels to manage the phase lag while maintaining robust performance against measurement noise and parameter variations.

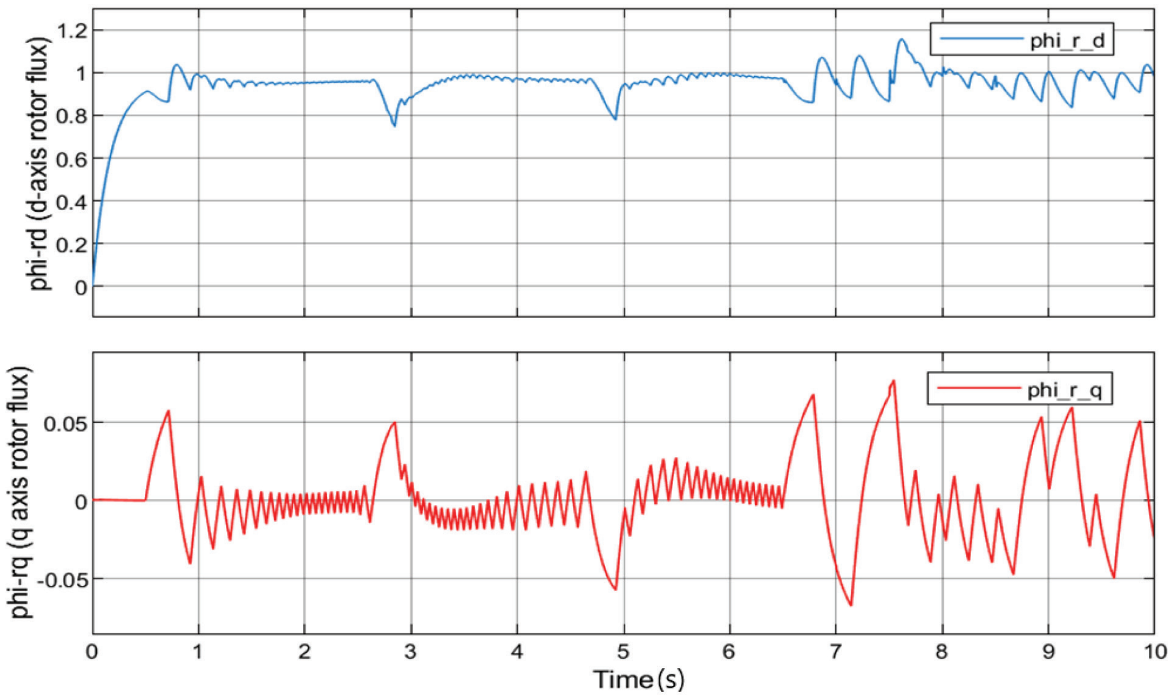

Figure 4. Rotor fluxes in d–q reference frame.

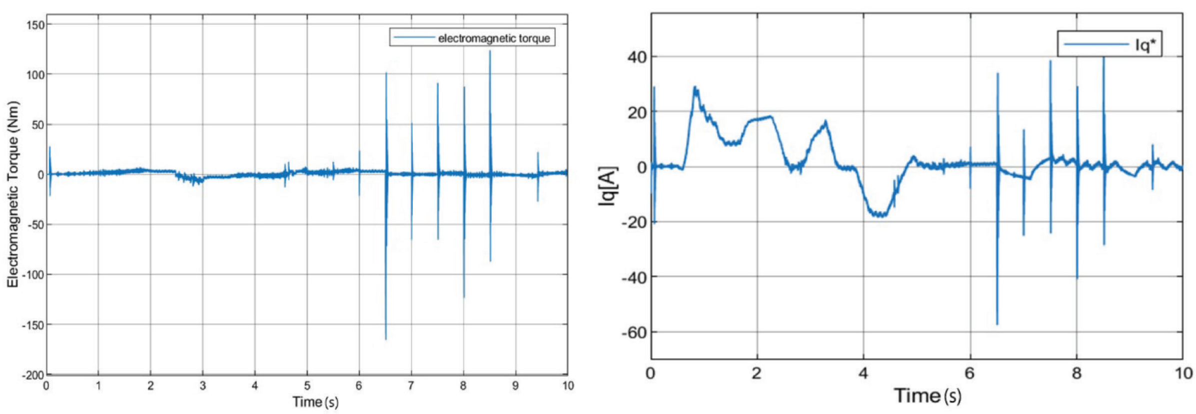

Figure 5. Electromagnetic torque (on the left) and the commanded stator current on the q-axis (on the right).

At higher noise levels, the observer's gain exponent is increased, allowing for a quicker response and better disturbance rejection, while at lower noise levels, the gain is decreased to ensure smooth and stable operation.

This adaptive tuning compensates for the phase delay introduced by the SOGI and enhances the observer's alignment with the actual rotor flux reference frame. As a result, the proposed approach achieves reliable speed and flux estimation across various operating conditions, ensuring precise and stable control in sensorless induction motor applications.

7.1. Performance of the proposed SOGI-HOSM as compared to the conventional SOGI-FLL and conventional STA under varying load torque and no additional sensor noise and no parameter variation

The performance of the proposed SOGI-HOSM was compared to the conventional SOGI-FLL and the conventional STA, the same load torque command was used in Figure 2. The proposed SOGI-HOSM, as shown in Figure 7,

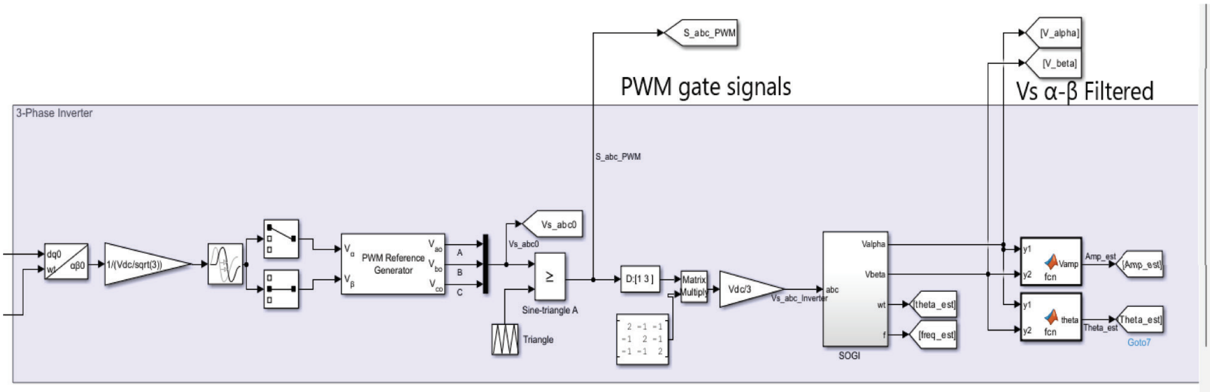

Figure 6. MATLAB/Simulink implementation of the filtering of $\hat{v}_\alpha$ and $\hat{v}_\beta$ by the SOGI topology. SOGI, second-order generalised integrator.

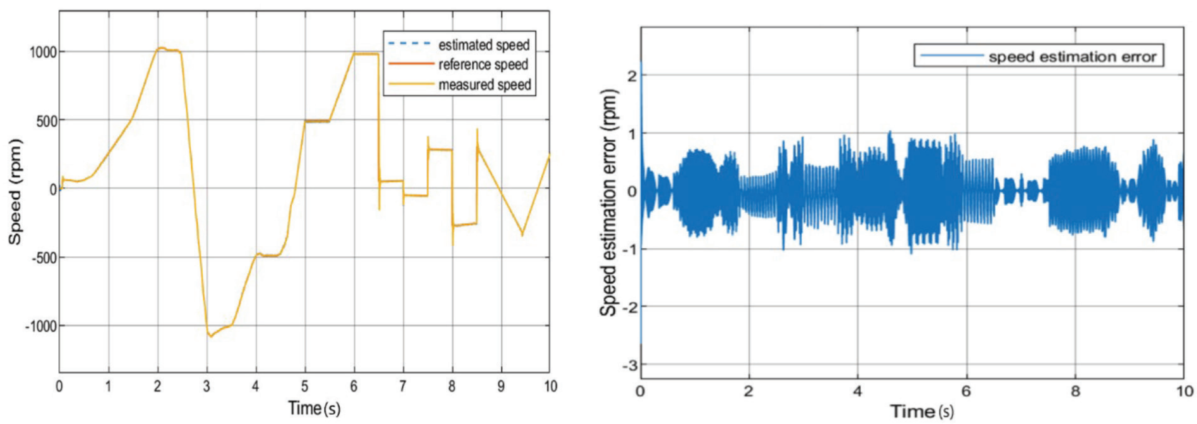

Figure 7. Performance of the proposed SOGI-HOSM at varying speed commands. SOGI-HOSM, second-order generalised integrator-higher-order sliding mode.

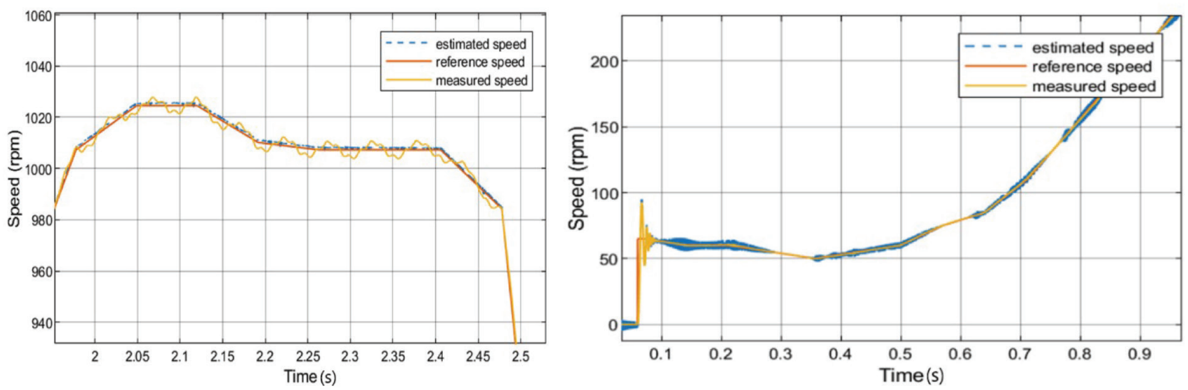

Figure 8. Zoomed-in version of the performance of the proposed SOGI-HOSM during frequency ramps (on the left) and at low speeds (on the right). SOGI-HOSM, second-order generalised integrator-higher-order sliding mode.

performed better than the conventional STA in Figure 10 and the conventional SOGI-FLL in Figure 12 with a maximum estimation error of ±1 rpm as compared to that of the STA: ±5 rpm and that of SOGI-FLL: ±1.5 rpm.

The proposed SOGI-HOSM system significantly improves speed estimation robustness and reduces chattering, as demonstrated in Figures 8 and 9, compared to the conventional STA in Figure 11. The conventional STA

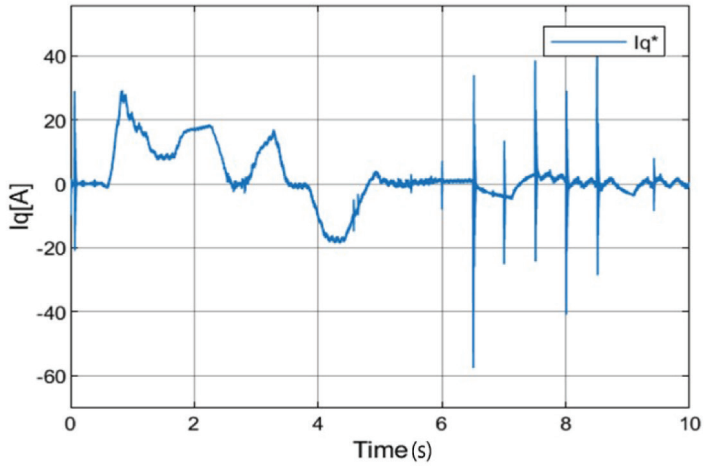

Figure 9. Current control command showing very little chattering using the proposed the SOGI-HOSM. SOGI-HOSM, second-order generalised integrator-higher-order sliding mode.

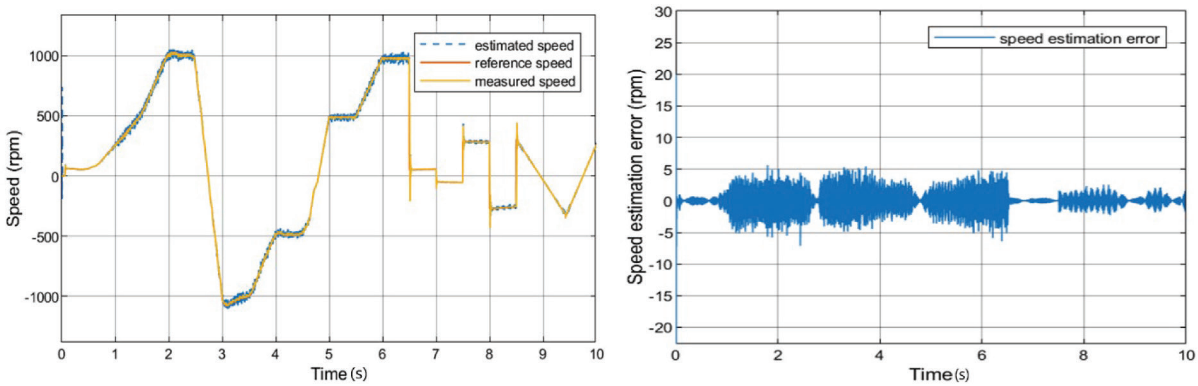

Figure 10. Performance of the conventional STA at varying speeds. STA, super-twisting algorithm.

experiences severe chattering, particularly during motor acceleration and at low speeds, due to the discontinuous signum function utilised in its design. This abrupt switching introduces high-frequency oscillations (chattering) that degrade performance and impact overall system stability. In contrast, the proposed SOGI-HOSM employs a hyperbolic tangent function, which ensures smoother transitions and effectively mitigates chattering while maintaining robust performance, even under dynamic operating conditions. This improvement results in enhanced stability and precision, particularly in low-speed regions where conventional methods often fail.

Additionally, the SOGI-HOSM system addresses the speed estimation degradation commonly observed in SOGI-based observers during frequency ramps, such as motor acceleration and deceleration. According to Wang et al. (2021), SOGI observers struggle during rapid speed changes due to their sensitivity to phase lag. This issue is evident in the conventional SOGI-FLL results shown in Figure 14, where estimation errors and lag become pronounced during these transitions. The proposed SOGI-HOSM system resolves these limitations through its dynamic gain tuning mechanism, which adjusts the gain exponent α in real-time based on noise levels. This adaptive mechanism allows the observer to dynamically minimise errors, maintain stability and deliver accurate speed estimation throughout frequency ramps, as illustrated in Figure 8.

By combining the noise-suppressing capabilities of the SOGI with the advanced chattering-reduction properties of the HOSM, the proposed system delivers superior performance compared to conventional STA and SOGI-FLL observers. These improvements are especially critical in applications requiring precision during dynamic conditions, such as variable-speed motor drives.

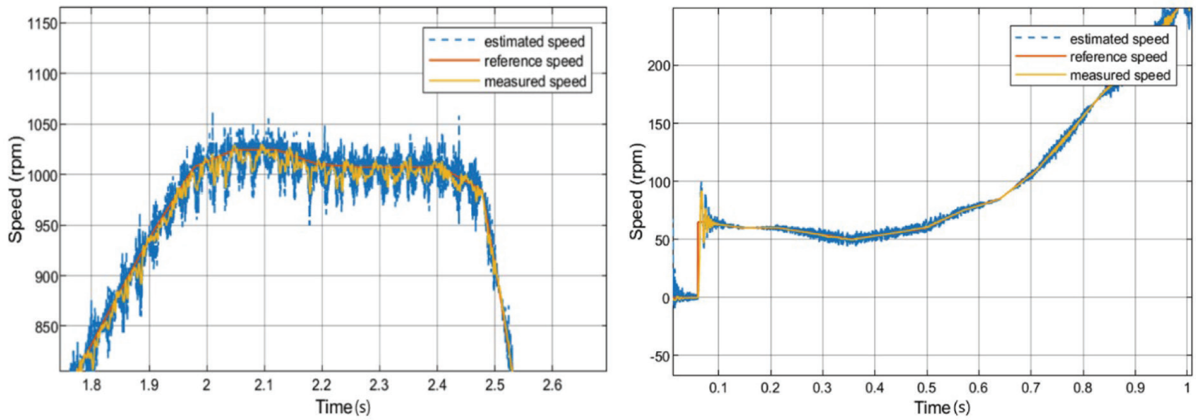

Figure 11. A zoomed-in version of the performance of the conventional STA during frequency ramps (on the left) and at low speeds (on the right). STA, super-twisting algorithm.

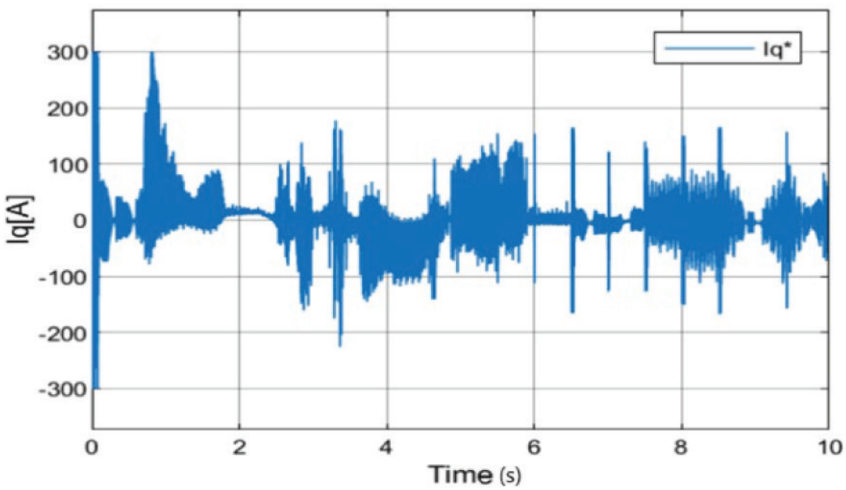

Figure 12. Current control command showing very large chattering using the conventional STA. STA, super-twisting algorithm.

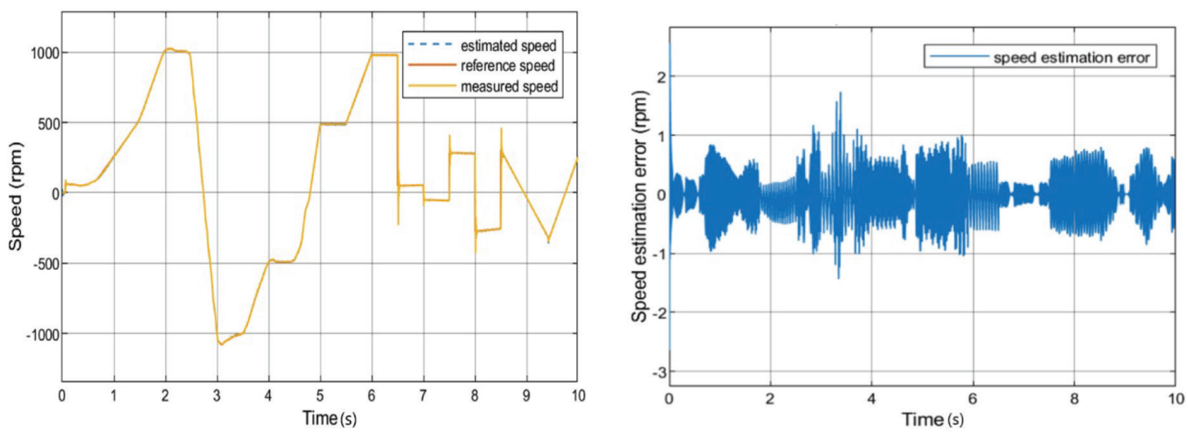

Figure 13. Performance of the conventional SOGI-FLL at varying speeds. SOGI-FLL, second-order generalised integrator-frequency locked loop.

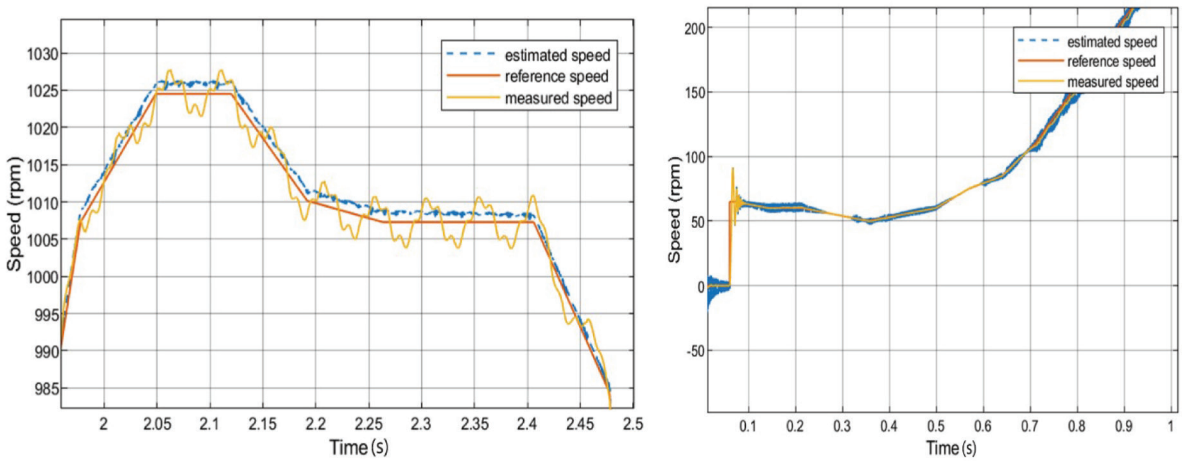

Figure 14. A zoomed-in version of the performance of the conventional SOGI-FLL at during frequency ramps (on the left) and at low speeds (on the right). SOGI-FLL, second-order generalised integrator-frequency locked loop.

Table 2. Parameter variation and noise level.

	Parameter	Variation (%)
ΔR_s	Stator resistance variation	+18
ΔL_s	Stator inductance variation	+10
ΔZ_n	Additional noise in current Sensor	±5

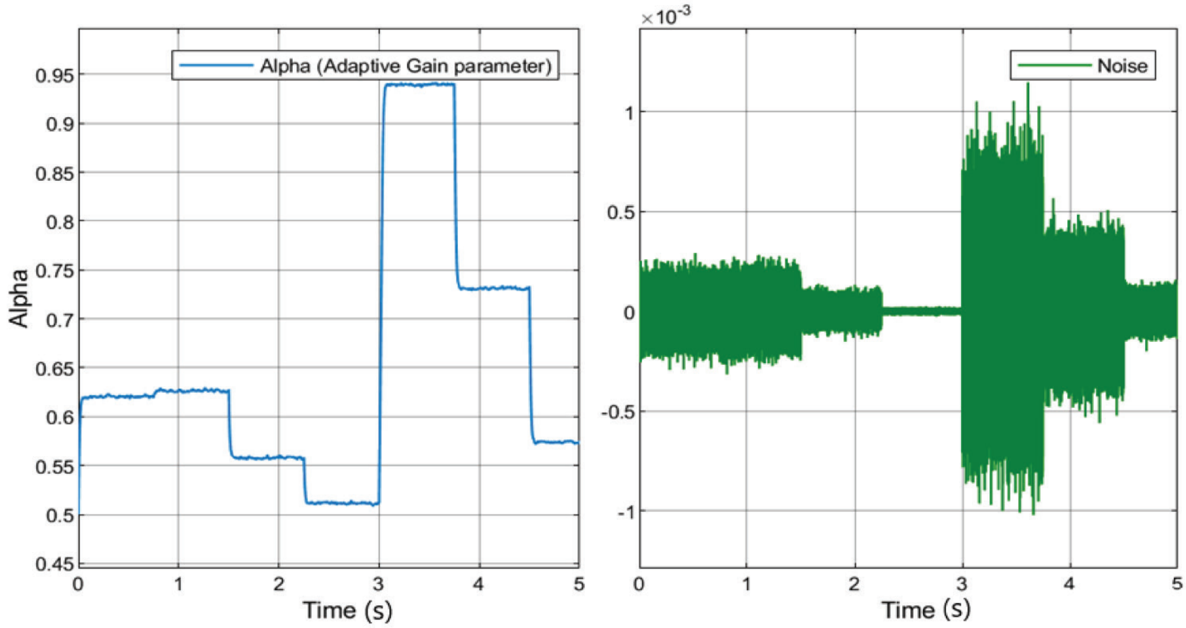

Figure 15. Gain varying according to the noise level from the Butterworth filter.

7.2. Performance of the proposed SOGI-HOSM compared to the conventional SOGI-FLL and conventional STA under varying load torque, additional sensor noise and parameter variation

High-frequency white noise was introduced into the feedback current signal at different levels while the induction motor model's parameters were simultaneously changed, along with the load torque to demonstrate the robustness

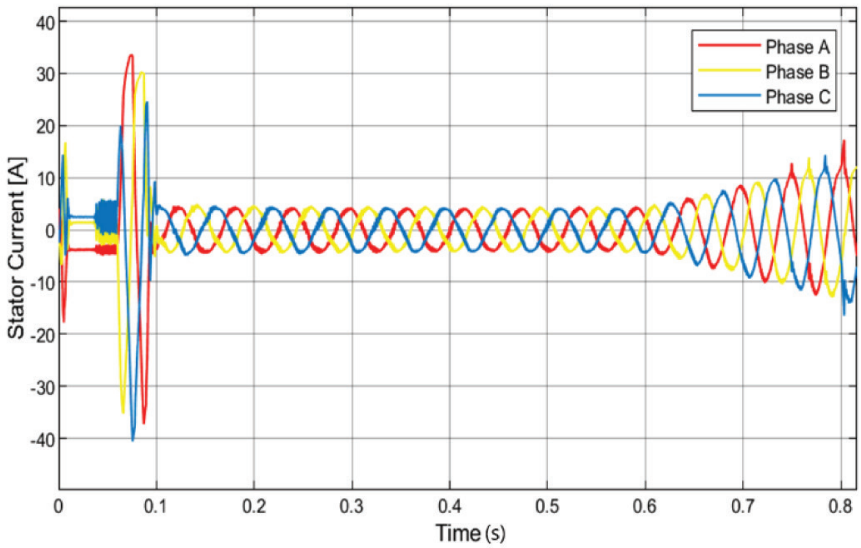

Figure 16. Phase currents of induction machine showing abnormal high sensor noise addition.

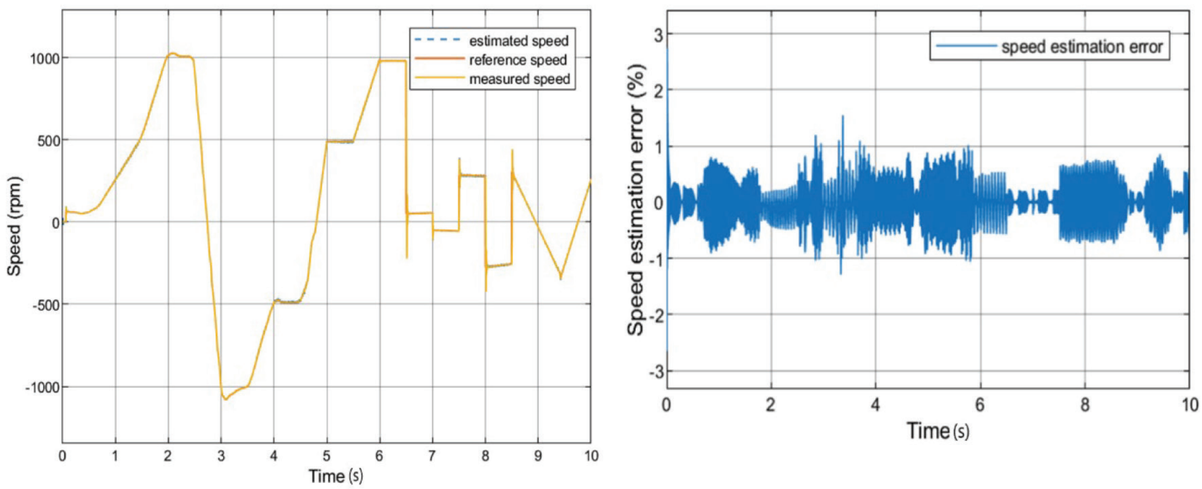

Figure 17. Performance of the proposed SOGI-HOSM under parameter variation, additional sensor noise and under varying load torque. SOGI-HOSM, second-order generalised integrator-higher-order sliding mode.

of the proposed SOGI-HOSM (the varying load torque used in Figure 2, is still being used here too). Figure 15 demonstrates the impressive fast change of alpha with a slight change in noise levels. The parameters varied and noise levels are demonstrated in Table 2. The Figure 16 shows the phase currents (A, B, and C) of the induction machine affected by high-frequency white noise added to the feedback signal.

7.2.1. Simulation results

The proposed SOGI-HOSM method outperforms the SOGI-FLL and STA with a maximum estimation error of ±1 rpm, as shown in Figure 17, as compared to STA: ±15 rpm, in Figure 19 and SOGI-FLL: ±5 rpm, in Figure 21. The performance enhancement of the proposed SOGI-HOSM system is significantly attributed to its dynamic adaptation of the alpha gain exponent (α), which adjusts in real-time based on the noise magnitude detected in the current sensor. This adaptive mechanism ensures the observer remains highly resilient to noise-induced disturbances, effectively compensating for their impact on speed estimation accuracy. By dynamically tuning α, the proposed method optimises the trade-off between noise rejection and responsiveness, maintaining robust and accurate

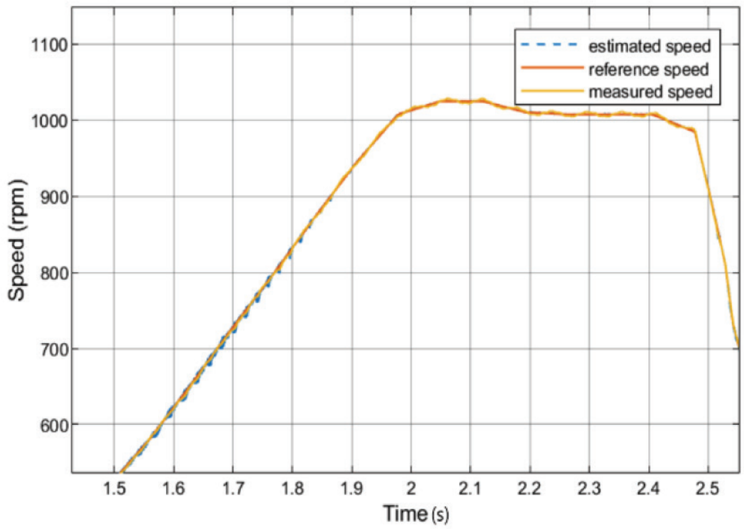

Figure 18. A zoomed-in version of the performance of the proposed SOGI-HOSM under parameter variation, additional sensor noise and under varying load torque. SOGI-HOSM, second-order generalised integrator-higher-order sliding mode.

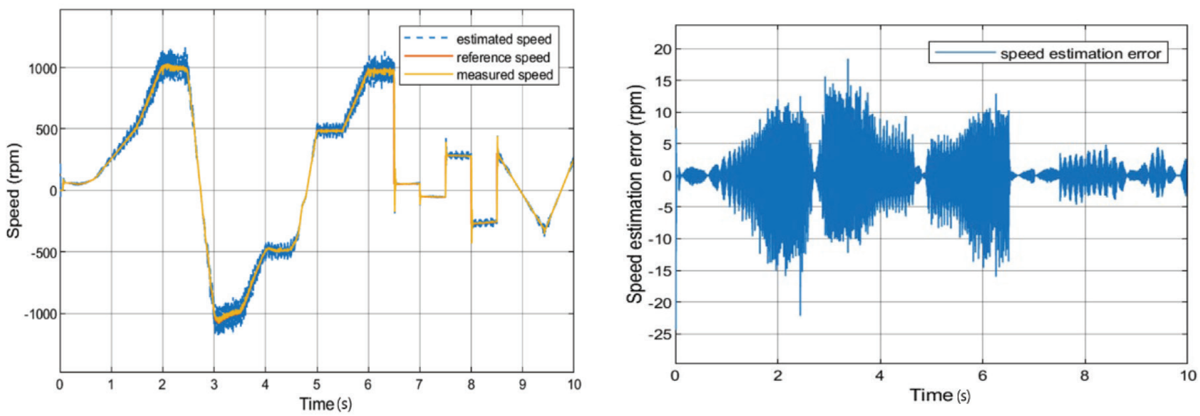

Figure 19. Performance of the STA method under parameter variation, additional sensor noise and under varying load torque. STA, super twisting algorithm.

speed estimation under challenging operating conditions such as parameter variations and the introduction of high-frequency white noise. This adaptability stabilises the system and mitigates the adverse effects of measurement noise, demonstrating its robustness against both noise and parameter deviations as shown in Figure 18.

When high-frequency white noise and parameter variations were introduced simultaneously, the SOGI-HOSM system significantly outperformed conventional methods, such as the SOGI-FLL and STA. Although the SOGI-FLL has good filtering capabilities, its inability to dynamically adjust to noise levels and parameter changes led to increased chattering and a noticeable degradation in speed estimation accuracy, as shown in Figure 22. This degradation underscores the limitations of the SOGI-FLL in noise-prone and dynamically varying environments.

The conventional STA also exhibited poor performance under noise and parameter variations, as depicted in Figure 20 and supported by literature (Mansouri et al., 2020). The STA's reliance on a discontinuous signum function amplified its sensitivity to noise, resulting in excessive chattering and significant errors in speed estimation. This chattering was particularly detrimental during transient conditions such as motor acceleration, deceleration and low-speed operation, where precise control is essential. Moreover, the STA's fixed alpha gain exponent ($\alpha = 0.5$) prevented it from adapting to varying noise levels, further exacerbating the chattering problem and degrading its performance.

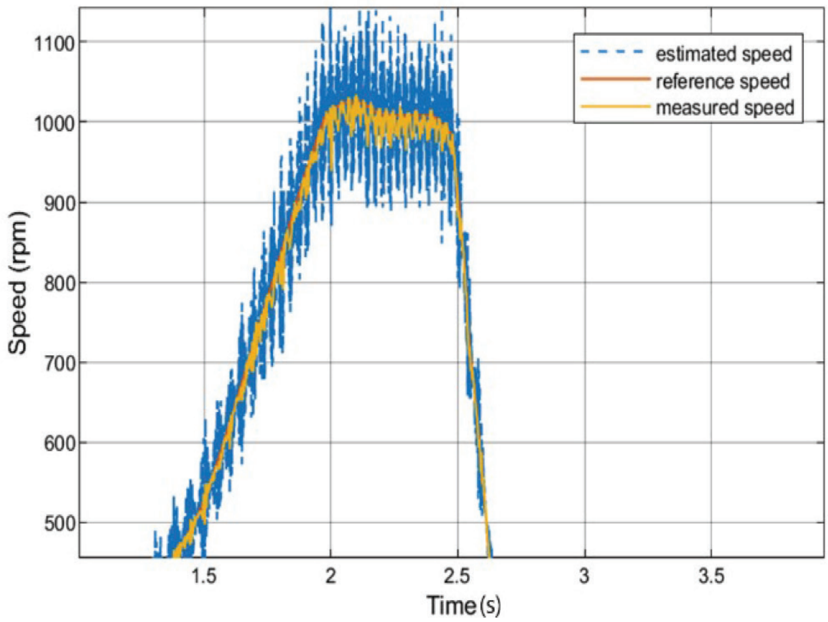

Figure 20. A zoomed-in version of the performance of the conventional STA under parameter variation, additional sensor noise and under varying load torque. STA, super twisting algorithm.

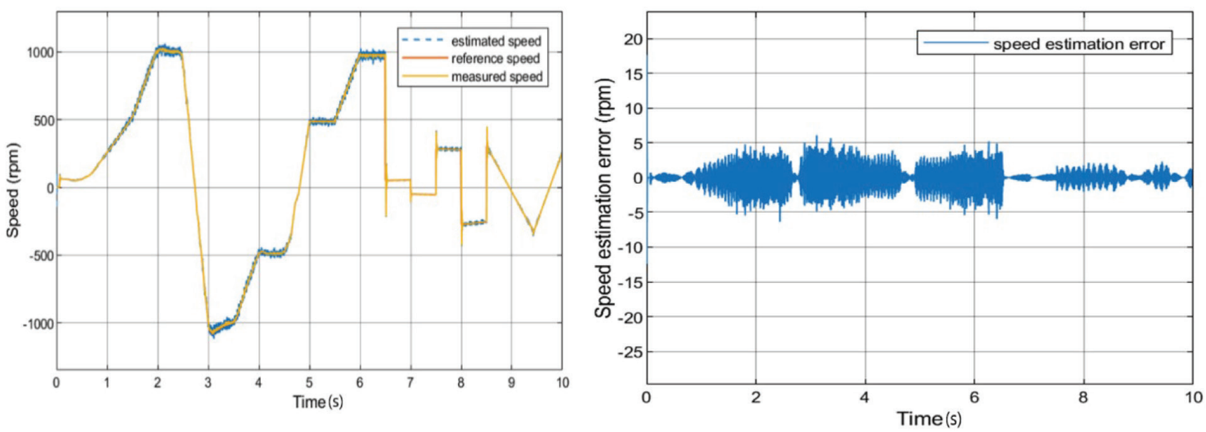

Figure 21. Performance of the SOGI-FLL method under parameter variation, additional sensor noise and under varying load torque. SOGI-FLL, second-order generalised integrator-frequency locked loop.

In contrast, the proposed SOGI-HOSM system combines a hyperbolic tangent function with a real-time gain tuning mechanism. The hyperbolic tangent function ensures smoother transitions, effectively mitigating chattering by replacing the abrupt switching caused by the signum function. Simultaneously, the dynamic gain tuning adjusts α between 0.5 and 1 based on noise magnitude, enabling the system to balance responsiveness and robustness. This combination allows the SOGI-HOSM to suppress chattering, maintain stability and ensure accurate speed estimation even in the presence of significant noise and parameter variations.

Simulation results highlight the SOGI-HOSM's superior performance, maintaining a maximum estimation error of ± 1 rpm under challenging conditions-a substantial improvement over the SOGI-FLL (±5 rpm) and STA (±15 rpm). These results, shown in Figures 20 and 22, reinforce the SOGI-HOSM's effectiveness in addressing the combined challenges of white noise and parameter variations. The SOGI-HOSM's advanced adaptive capabilities make it a superior solution for sensorless speed estimation in induction motor control, ensuring reliability and robustness where conventional methods fall short. Its practical advantages establish it as a reliable and efficient choice for demanding real-world applications.

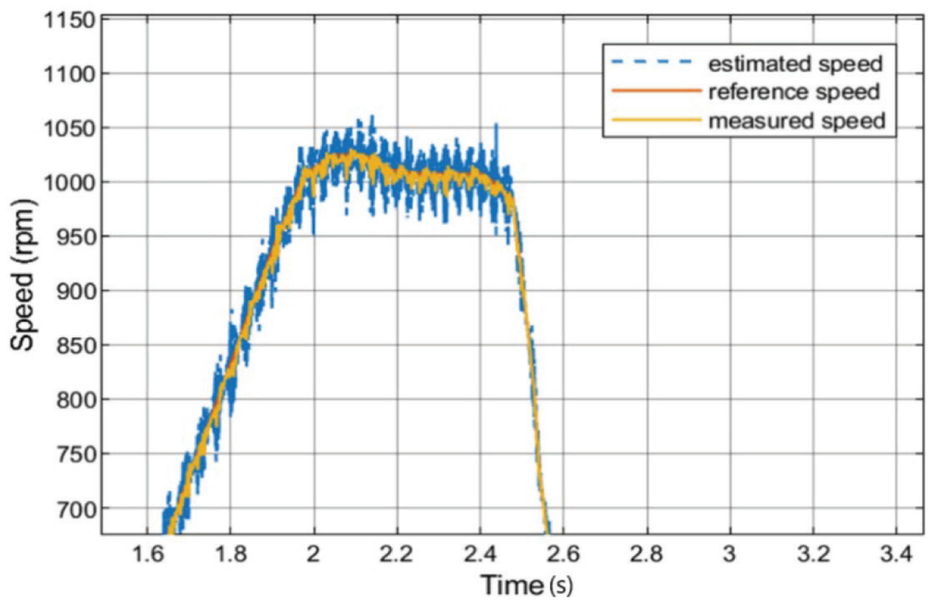

Figure 22. A zoomed-in version of the performance of the SOGI-FLL method under parameter variation, additional sensor noise and under varying load torque. SOGI-FLL, second-order generalised integrator-frequency locked loop.

8. Conclusion

This article introduces a novel adaptive gain tuning SOGI-HOSM observer for robust and accurate sensorless speed estimation of induction motors across their entire speed range. The proposed method dynamically adjusts the alpha gain exponent, enhancing its resilience to parameter variations, noise and load torque changes. A thorough stability and convergence analysis demonstrates its robustness, while simulation results confirm its superior performance compared to conventional methods like the SOGI-FLL and STA. By achieving lower estimation errors, reducing chattering and maintaining stable operation under challenging conditions, the SOGI-HOSM observer represents a significant advancement in sensorless speed estimation, offering a reliable and effective solution for real-world induction motor applications.

8.1. Limitations of the proposed SOGI-HOSM method

While the proposed SOGI-HOSM method demonstrates significant improvements in robustness and accuracy under various operating conditions, it is not without limitations. The adaptive gain tuning mechanism and dynamic adjustment of the alpha exponent increase computational complexity, potentially necessitating advanced processing hardware for real-time applications, which could limit its adoption in cost-sensitive scenarios. Additionally, although the method has been rigorously tested against high-frequency noise, its sensitivity to other noise types, such as thermal noise, electromagnetic interference (EMI) and vibration-induced noise, remains unexplored. Practical implementation may also present challenges, particularly in fine-tuning parameters like the alpha gain exponent to maintain stability across diverse operating conditions.

8.2. Future works

Future research on the proposed SOGI-HOSM method should focus on several key areas to enhance its robustness, applicability and practical implementation. First, comprehensive testing against a wider range of noise types, such as thermal noise, EMI, vibration-induced noise and shot noise, is essential to evaluate and improve its resilience under diverse environmental conditions. Second, physical implementation of the proposed method on a standard induction motor test bench is necessary to validate its performance and stability in real-world scenarios. This includes addressing practical challenges such as parameter tuning and hardware integration. Additionally, exploring ways to optimise the computational requirements of the algorithm will be crucial to ensure its feasibility for cost-sensitive applications.

References

Ammar, A., Belaroussi, O., Benakcha, M., Zemmit, A. and Ameid, T. (2024). Super-Twisting MRAS Observer-Based Non-linear Direct Flux and Torque Control for Induction Motor Drives. *Power Electronics and Drives*, 9, pp. 374–396. doi: 10.2478/pead-2024-0024

Bamigbade, A. and Khadkikar, V. (2022). Frequency Estimators for SOGI FLL: Modeling, Design, and Equivalence for FLL Advancements. *IEEE Transactions on Instrumentation and Measurement*, 71, pp. 1–12.doi: 10.1109/tim.2022.3210972

Bouzidi, R., Ghadbane, I., Boukhari, M., Bendib, A. and Kherbachi, A. (2022). Experimental Implementation of Low-Cost and Robust Sensorless Control based on SOGI-FLL Estimator for Electric Vehicles. *International Journal of Power Electronics and Drive Systems*, 13, p. 1993.doi: 10.11591/ijpeds.v13.i4.pp1993-2004.

Caruana, C., Asher, G. M. and Sumner, M. (2006). Performance of HF Signal Injection Techniques for Zero-Low-Frequency Vector Control of Induction Machines Under Sensorless Conditions. *IEEE Transactions on Industrial Electronics*, 53, pp. 225–238. doi: 10.1109/TIE.2005.862257

Echeikh, H., Trabelsi, R., Iqbal, A., Bianchi, N. and Mimouni, M. F. (2016). Comparative Study Between the Rotor Flux Oriented Control and Non-Linear Backstepping Control of a Five-Phase Induction Motor Drive – An Experimental Validation. *IET Power Electron*, 9, pp. 2510–2521. doi: 10.1049/iet-pel.2015.0726

Farahat, A., Liu, Z., Liu, G. and Chen, Q. (2024). Speed and Position Estimation for 5-ph PMSM Using SOGI Based on SMO Considering Short-Circuit Fault. *IEEE Access*, 12, pp. 57315–57325. doi: 10.1109/ACCESS.2024.3387284

Gao, Q., Asher, G. and Sumner, M. (2007). Sensorless Position and Speed Control of Induction Motors Using High-Frequency Injection and Without Offline Precommissioning. *IEEE Transactions on Industrial Electronics*, 54, pp. 2474–2481. doi: 10.1109/TIE.2007.90036

Gao, Z., Turner, L., Colby, R. S. and Leprettre, B. (2011). A Frequency Demodulation Approach to Induction Motor Speed Detection. *IEEE Transactions on Industry Applications*, 47, pp. 1632–1642. doi: 10.1109/TIA.2011.2153813

Ghanes, M., Moreno, J. A. and Barbot, J.-P. (2022). Arbitrary Order Differentiator with Varying Homogeneity Degree. *Automatica*, 138, pp. 110111. doi: 10.1016/j.automatica.2021.110111

Golestan, S., Guerrero, J. M. and Vasquez, J. C. (2016). Three-Phase PLLs: A Review of Recent Advances. *IEEE Transactions on Power Electronics*, 32, pp. 1894–1907. doi: 10.1109/TPEL.2016.2565642

Golestan, S., Guerrero, J. M. and Vasquez, J. C. (2017). Single-Phase PLLs: A Review of Recent Advances. *IEEE Transactions on Power Electronics*, 32, pp. 9013–9030. doi: 10.1109/TPEL.2017.2653861

Hao, X. and Luo, Y. (2024). Research on TOGI-EFLL Flux Observer for IPMSM Sensorless Control. *IET Power Electronics*, 17, pp. 1806–1819. doi: 10.1049/pel2.12735

Holtz, J. (1998). Sensorless position control of induction motors. An emerging technology. In: *AMC'98-Coimbra. 1998 5th International Workshop on Advanced Motion Control. Proceedings* (Cat. No. 98TH8354). IEEE, pp. 1–14.

Holtz, J. (2002). Sensorless Control of Induction Motor Drives. *Proceedings of the IEEE*, 90, pp. 1359–1394. doi: 10.1109/JPROC.2002.800726

Holtz, J. (2006). Sensorless Control of Induction Machines – With or Without Signal Injection? *IEEE Transactions on Industrial Electronics*, 53, pp. 7–30. doi: 10.1109/TIE.2005.862324

Ilas, C., Bettini, A., Ferraris, L., Griva, G. and Profumo, F. (1994). Comparison of different schemes without shaft sensors for field oriented control drives. In: *Proceedings of IECON'94-20th Annual Conference of IEEE Industrial Electronics*. IEEE, pp. 1579–1588.

Jansen, P. L. and Lorenz, R. D. (1993). Accuracy limitations of velocity and flux estimation in direct field oriented induction machines. In: *1993 Fifth European Conference on Power Electronics and Applications. Presented at the 1993 Fifth European Conference on Power Electronics and Applications*, Vol. 4, pp. 312–318.

Khoshhava, M. A., Zarchi, H. A. and Markadeh, G. A. (2021). Sensor-Less Speed and Flux Control of Dual Stator Winding Induction Motors Based on Super Twisting Sliding Mode Control. *IEEE Transactions on Energy Conversion*, 36, pp. 3231–3240. doi: 10.1109/TEC.2021.3077829

Leppanen, V.-M. and Luomi, J. (2006). Observer Using Low-Frequency Injection for Sensorless Induction Motor Control-Parameter Sensitivity Analysis. *IEEE Transactions on Industrial Electronics*, 53, pp. 216–224. doi: 10.1109/TIE.2005.862293

Mansouri, S. A., Ahmarinejad, A., Javadi, M. S., Heidari, R. and Catalão, J. P. S. (2020). Improved

Double-Surface Sliding Mode Observer for Flux and Speed Estimation of Induction Motors. *IET Electric Power Applications*, 14, pp. 1002–1010. doi: 10.1049/iet-epa.2019.0826

Nurettin, A. and İnanç, N. (2023). Sensorless Vector Control for Induction Motor Drive at Very Low and Zero Speeds Based on an Adaptive-Gain Super-Twisting Sliding Mode Observer. *IEEE Journal of Emerging and Selected Topics in Power Electronics*, 11, pp. 4332–4339. doi: 10.1109/JESTPE.2023.3265352

Polyakov, A. and Poznyak, A. (2009). Lyapunov Function Design for Finite-Time Convergence Analysis: "Twisting" Controller for Second-Order Sliding Mode Realization. *Automatica*, 45, pp. 444–448. doi: 10.1016/j.automatica.2008.07.013

Raute, R., Caruana, C., Staines, C. S., Cilia, J., Sumner, M. and Asher, G. M. (2010). Sensorless Control of Induction Machines at Low and Zero Speed by Using PWM Harmonics for Rotor-Bar Slotting Detection. *IEEE Transactions on Industry Applications*, 46, pp. 1989–1998. doi: 10.1109/TIA.2010.2057495

Sun, X., Wang, N., Yao, M. and Lei, G. (2024). Position Sensorless Control of SRMs Based on Improved Sliding Mode Speed Controller and Position Observer. *IEEE Transactions on Industrial Electronics*, 72(1), pp. 100–110. doi: 10.1109/tie.2024.3398685

Traore, D., De Leon, J., Glumineau, A. and Loron, L. (2007). Speed Sensorless Field-Oriented Control of Induction Motor with Interconnected Observers: Experimental Tests on Low Frequencies Benchmark. *IET Control Theory and Applications*, 1, pp. 1681–1692. doi: 10.1049/iet-cta:20060453

Veluvolu, K. C. and Soh, Y. C. (2009). High-Gain Observers with Sliding Mode for State and Unknown Input Estimations. *IEEE Transactions on Industrial Electronics*, 56, pp. 3386–3393. doi: 10.1109/TIE.2009.2023636

Wang, G., Li, Z., Zhang, G., Yu, Y. and Xu, D. (2012). Quadrature PLL-Based High-Order Sliding-Mode Observer for IPMSM Sensorless Control with Online MTPA Control Strategy. *IEEE Transactions on Energy Conversion*, 28, pp. 214–224. doi: 10.1109/TEC.2012.2228484

Wang, G., Zhan, H., Zhang, G., Gui, X. and Xu, D. (2013). Adaptive Compensation Method of Position Estimation Harmonic Error for EMF-Based Observer in Sensorless IPMSM Drives. *IEEE Transactions on Power Electronics*, 29, pp. 3055–3064. doi: 10.1109/TPEL.2013.2276613

Wang, H., Yang, Y., Ge, X., Zuo, Y., Yue, Y. and Li, S. (2021). PLL-and FLL-Based Speed Estimation Schemes for Speed-Sensorless Control of Induction Motor Drives: Review and New Attempts. *IEEE Transactions on Power Electronics*, 37, pp. 3334–3356. doi: 10.1109/TPEL.2021.3117697

Wang, T., Wang, B., Yu, Y., Xu, D. (2024). A Closed-Loop Voltage Model Observer for Sensorless Induction Motor Drives Based on the Orthogonality and Sliding-Mode Technique. *IEEE Trans. Ind. Electron*. 71, pp. 13693–13707. doi: 10.1109/TIE.2024.3374363

Xin, Z., Zhao, R., Blaabjerg, F., Zhang, L. and Loh, P. C. (2016). An Improved Flux Observer for Field-Oriented Control of Induction Motors Based on Dual Second-Order Generalized Integrator Frequency-Locked Loop. *IEEE Journal of Emerging and Selected Topics in Power Electronics*, 5, pp. 513–525. doi: 10.1109/JESTPE.2016.2623668

Zaky, M.S., Khater, M.M., Shokralla, S.S., Yasin, H.A. (2009). Wide-Speed-Range Estimation With Online Parameter Identification Schemes of Sensorless Induction Motor Drives. *IEEE Trans. Ind. Electron*. 56, pp. 1699–1707. doi: 10.1109/TIE.2008.2009519

Zhao, L., Huang, J., Chen, J. and Ye, M. (2015). A Parallel Speed and Rotor Time Constant Identification Scheme for Indirect Field Oriented Induction Motor Drives. *IEEE Transactions on Power Electronics*, 31, pp. 6494–6503. doi: 10.1109/TPEL.2015.2504399

Zhao, R., Xin, Z., Loh, P. C. and Blaabjerg, F. (2016). A Novel Flux Estimator Based on Multiple Second-Order Generalized Integrators and Frequency-Locked Loop for Induction Motor Drives. *IEEE Transactions on Power Electronics*, 32, pp. 6286–6296. doi: 10.1109/TPEL.2016.2620428